

# SHAPE, SPIN AND BARYON FRACTION OF CLUSTERS IN THE MARENOSTRUM UNIVERSE

STEFAN GOTTLÖBER

Astrophysikalisches Institut Potsdam, An der Sternwarte 16, 14482 Potsdam, Germany

AND

GUSTAVO YEPES

Grupo de Astrofísica, Universidad Autónoma de Madrid, Madrid E-28049, Spain

*Draft version September 28, 2018*

## ABSTRACT

The *MareNostrum Universe* is one of the largest cosmological SPH simulation done so far. It consists of  $1024^3$  dark and  $1024^3$  gas particles in a box of  $500 h^{-1}$  Mpc on a side. Here we study the shapes and spins of the dark matter and gas components of the 10,000 most massive objects extracted from the simulation as well as the gas fraction in those objects. We find that the shapes of objects tend to be prolate both in the dark matter and gas. There is a clear dependence of shape on halo mass, the more massive ones being less spherical than the less massive objects. The gas distribution is nevertheless much more spherical than the dark matter, although the triaxiality parameters of gas and dark matter differ only by a few percent and it increases with cluster mass. The spin parameters of gas and dark matter can be well fitted by a lognormal distribution function. On average, the spin of gas is 1.4 larger than the spin of dark matter. We find a similar behavior for the spins at higher redshifts, with a slightly decrease of the spin ratios to 1.16 at  $z = 1$ . The cosmic normalized baryon fraction in the entire cluster sample ranges from  $Y_b = 0.94$ , at  $z = 1$  to  $Y_b = 0.92$  at  $z = 0$ . At both redshifts we find a slightly, but statistically significant decrease of  $Y_b$  with cluster mass.

*Subject headings:* cosmology:theory – clusters:general – methods:numerical

## 1. INTRODUCTION

According to the standard scenario cosmic structures form by the gravitational collapse of density fluctuations. This collapse is mainly determined by the dark matter (DM) which contributes 85% to the total matter density in the universe. Baryonic matter follows the DM and forms visible objects like galaxies and clusters inside the DM halos.

Shape and angular momentum are two important characteristics of halos. The shape of DM halos has been already widely studied, mainly by means of N-body simulations (e.g. Allgood et al. (2006), Macciò et al (2006), Bett et al (2006) and references therein). Avila-Reese et al. (2005) discuss the dependence of the shape of galaxy sized halos on environment. Bailin & Steinmetz (2005) studied the internal shape of DM halos. Clusters of galaxies are the most recently formed objects in the universe. Most of the gas has not had time to cool. Since gas contributes only 15 % of the total mass one would expect that the gas follows DM and both distribution should be similar. In order to quantify this similarity, we have characterized the shape of both components in halos obtained from a large non-radiative cosmological gasdynamical simulation. Further we have compared the baryon fraction in clusters with the cosmic baryon fraction.

The origin, evolution and distribution of DM halo spins have been widely discussed in the past also (eg. Vitvitska et al. (2002), Bullock et al. (2001), Macciò et al (2006), Bett et al (2006)). In galactic size halos the angular momentum of the gas component is important for the understanding of disk formation. Using

gasdynamical simulations van den Bosch et al. (2002), Chen, Jing, & Yoshikaw (2003), Sharma & Steinmetz (2005) have studied the spin of the gas component in galactic halos and found that at redshift  $z = 0$  the gas component, on average, has a larger spin than DM. Here we will discuss briefly the relation between the different definitions of the spin parameter and study the distribution of spin parameters of DM and gas components in our numerical clusters.

Most of the previous studies on shape and spin of halos used either collisionless dark matter simulations with large number of particles and relatively large volumes or gasdynamical (dissipative and non dissipative) simulations in small volumes with a small number of objects. The advantage of our study is that we have both gas and dark matter components in the MareNostrum SPH simulation and a large cluster sample (more than 10,000) to perform statistics, thanks to the large computational volume and the high number of particles of this simulation.

## 2. NUMERICAL SIMULATION

This simulation, dubbed THE MARENOSTRUM UNIVERSE, was performed with the entropy conserving GADGET2 code (Springel 2005) on the MareNostrum supercomputer at the Barcelona Supercomputer Center using the equivalent of about 29 years on a single CPU. It followed the non linear evolution of structures in gas and dark matter (DM) from  $z = 40$  to the present epoch ( $z = 0$ ) within a comoving cube of  $500h^{-1}$ Mpc edges. We assumed the spatially flat concordance cosmological model with the following parameters: the total matter density  $\Omega_m = 0.3$ , the baryon density  $\Omega_b = 0.045$ , the cosmological constant  $\Omega_\Lambda = 0.7$ , the Hubble parameter  $h = 0.7$ , the slope of the initial power spectrum  $n = 1$

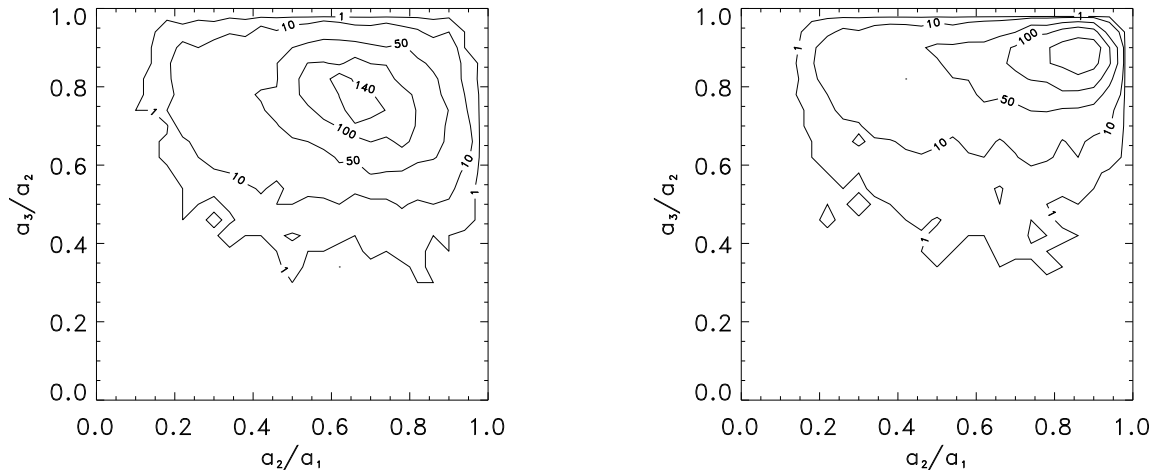


FIG. 1.— *Left*: Shape of the dark matter distribution in clusters with total masses larger than  $5 \times 10^{13} h^{-1} M_{\odot}$ ,  $a_1$ ,  $a_2$ ,  $a_3$  are the three main axes of the clusters. *Right*: The same for the shape of the gas distribution.

and the normalization  $\sigma_8 = 0.9$ . The power spectrum used to generate the initial conditions for the simulation was kindly provided by Wayne Hu in a tabulated form. It was obtained from a direct integration of the Boltzmann code for the parameters described above. We did numerical interpolation to compute the contribution of the different Fourier modes. Both components, the gas and the DM, were resolved by  $1024^3$  particles, which resulted in a mass of  $8.3 \times 10^9 h^{-1} M_{\odot}$  for the DM particles and  $1.5 \times 10^9 h^{-1} M_{\odot}$  for the gas particles, respectively.

GADGET2 uses the TREEPM algorithm on a homogeneous Eulerian grid to compute large scale forces by the Particle-Mesh algorithm. In this simulation we employed  $1024^3$  mesh points to compute the density field from particle positions and FFT to derive gravitational forces. Within GADGET2 the equations of gas dynamics are solved by means of the Smoothed Particle Hydrodynamics (SPH) method in its entropy conservation scheme. We did not include dissipative or radiative processes or star formation. The spatial force resolution was set to an equivalent Plummer gravitational softening of  $15 h^{-1}$  comoving kpc. The SPH smoothing length was set to the distance to the  $40^{th}$  nearest neighbor of each SPH particle.

The MARENOSTRUM UNIVERSE is part of a series of simulations we have performed during the last years. To this end, we had generated a realization of the  $\Lambda$ CDM power spectrum with  $2048^3$  particles and then decreased the mass resolution in the whole box to  $256^3$ ,  $512^3$  and  $1024^3$  particles respectively. The lower resolution ( $2 \times 256^3$ ,  $2 \times 512^3$ ) SPH simulations have been used to study properties of galaxy clusters (Yepes et al. 2004) and the shape-alignment relation of clusters (Faltenbacher et al. 2005; Basilakos et al. 2006). The MareNostrum Universe have been recently used to analyzed the entropy profiles of the gas and DM in galaxy clusters (Faltenbacher et al. 2006). Due to computational limitations, we could not yet simulate the evolution of the full box with the maximal possible resolution of the initial conditions,  $2 \times 2048^3$  particles. However, using the multi mass technique described in Klypin et al. (2001) selected individual clus-

ters have already been re-simulated at this resolution (Ascasibar et al. 2006).

It is a challenge to find within a distribution of 2 billion particles all structures and substructures and to determine their properties. Here we have used a newly developed parallel version of the hierarchical friends-of-friends (FOF) algorithm (Klypin et al. 1999). In a first step we construct the minimum spanning tree for the distribution of gas and DM particles. After topological sorting we get a cluster-ordered sequence from which we can easily extract FOF clusters by simple cutting the tree at the desired linking length. We use a basic linking length of 0.17 of the mean interparticle separation to extract the FOF clusters (Gottlöber et al. 2006b). We divide this linking length by  $2^n$  ( $n = 1, 3$ ) to find substructures and in particular the centers (density peaks) of our objects. We were running the minimum spanning tree and the FOF analysis independently over DM and gas particles to find their distribution. Using a linking length of 0.17 at redshift  $z = 0$  we have identified more than 2 million objects with more than 20 DM particles which closely follow a Sheth-Tormen mass function (Gottlöber et al. 2006a).

To determine the shape and spin of the clusters we have selected a subsample of more than 10,000 clusters and groups with masses larger than  $5 \times 10^{13} h^{-1} M_{\odot}$ . The lower mass threshold corresponds to clusters resp. massive groups with about 5000 gas particles and 5000 dark matter particles. As mentioned above the objects were identified independently from the gas and DM distributions. Due to the large number of particles in this simulation we can unambiguously match DM and gas halos with the same center of mass to one cluster. In the following we will study these two components of the clusters in more detail.

### 3. SHAPES

Using the FOF method one extracts rather complex objects from the simulation which are characterized by an iso-density surface given by the linking length. In first approximation these objects can be characterized

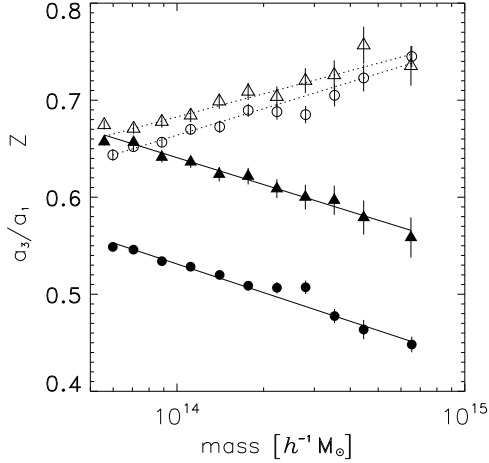


FIG. 2.— Ratio of the minor to major axes  $a_3/a_1$  (filled symbols) and triaxiality parameter  $Z$  (open symbols) for the DM (circles) and gas (triangles) distribution in our numerical clusters

by three-axial ellipsoids. The shape and orientation of the ellipsoids can be directly calculated as eigenvectors of the inertia tensor of the given object. Then the shape is characterized by the ratios between the lengths of the axes  $a_1 \geq a_2 \geq a_3$ .

We ran the FOF algorithm independently over the DM and gas particles to determine the shape of the distribution of the two components. In Fig. 1 we show the shape of the dark matter and gas distribution in clusters with total masses larger than  $5 \times 10^{13} h^{-1} M_\odot$ . The ratios  $a_3/a_2$  and  $a_2/a_1$  of the clusters have been sampled into 25 bins of size 0.04. The plot shows a clear difference between the shapes of DM (left) and gas (right) distribution. DM halos are centered at ratios (0.7, 0.75) whereas for the gas halos the center is at (0.85, 0.9), (*i.e.* the gas halos are much more spherical). Both shapes tend to be more prolate, *i.e.*  $a_3/a_2 > a_2/a_1$ . This could be the result of merging along a preferred direction, the large scale filaments (Faltenbacher et al. 2005).

The exact position of the maximum in left and right panel of Fig. 1 depends on the low mass cut-off in the cluster sample, but the qualitative behavior is independent of it. In 2, we show how the ratio of the minor to major axis  $a_3/a_1$  of DM (filled circles) and gas (filled triangles) halos depend on cluster mass. Note, that the dispersion in the values of the ratios  $a_3/a_1$  is large (within one bin the  $1\sigma$  scatter is 0.14). This can be seen in Fig. 1 for the ratios  $a_2/a_1$  and  $a_3/a_2$ . However, due to the large number of objects per mass bin the standard deviation of the average within each bin shown in Fig. 2 is small and sometimes smaller than the symbol size. The solid line is a linear fit in the semi-logarithmic plot  $a_3/a_1 = b + c \ln(M)$ , where the mass  $M$  is given in  $h^{-1} M_\odot$  and  $b$  and  $c$  are (1.904, -0.0426) and (1.932, -0.0401) for DM and gas, respectively. A similar trend (but higher  $a_3/a_1$  have been found by Kasun & Evrard (2005) in the Hubble Volume N-body simulation.

The cluster shape can be further characterized by the triaxiality parameter  $Z = (a_1 - a_2)/(a_1 - a_3)$  introduced by Binney (1985).  $Z = 1$  corresponds to prolate ellipsoids of revolution (prolate spheroids), while  $Z = 0$  corresponds to oblate ones. In Fig. 2 the triaxiality param-

eter  $Z$  is shown for the DM (open circles) and gas halos (open triangles). The dotted line is a fit  $Z = d + f \ln(M)$  with  $(d, f) = (-0.61, 0.039)$  for DM and  $(-0.43, 0.034)$  for gas halos. Contrary to the ratio  $a_3/a_1$  there is only little difference between the triaxiality parameter  $Z$  of the DM and gas halos. The younger the halos are (*i.e.* more massive) the more prolate they look.

#### 4. SPIN

In N-body numerical simulations the identified clusters can be characterized by their mass velocity and angular momentum or spin. Originally the spin parameter  $\lambda$  was introduced by Peebles (1971) as the “convenient dimensionless number”

$$\lambda = \frac{J|E|^{1/2}}{GM^{5/2}}, \quad (1)$$

where  $J$  is the total angular momentum of the object,  $E$  its total energy and  $M$  its mass. Following Padmanabhan (1993) one can interpret  $\lambda$  as the ratio of the angular velocity  $\omega$  of the system to the angular velocity  $\omega_{\text{sup}}$  of the system that would provide rotational support. Characterizing the system by its angular momentum  $J \simeq \omega MR^2$  and rotational support by  $\omega_{\text{sup}}^2 R^2 \simeq GM/R$  one finds

$$\lambda = \frac{\omega}{\omega_{\text{sup}}} = \frac{J}{G^{1/2} M^{3/2} R^{1/2}}, \quad (2)$$

which is up to a factor of  $\sqrt{2}$  Bullock’s  $\lambda'$  (Bullock et al. 2001) if one replaces  $GM/R$  by the circular velocity  $V_{\text{circ}}^2$ . Contrary to Eq.(1) both Bullock’s definition and Eq.(2) contain only quantities which can be easily calculated in numerical simulations for spherical halos. If we assume that the total energy of the system is characterized by  $E \simeq -GM^2/R$  one comes back to Peebles’ original definition.

The halos in the numerical simulation are assumed to be virialised and thus characterized by  $2T + U = 0$ , where  $T$  and  $U$  are the kinetic and potential energies of the object. Bett et al (2006) show in their Fig. 5 how real halos scatter around this assumption. Replacing the potential energy in Eq.(1) by  $(-2T)$  we end up with a third definition of the spin parameter:

$$\lambda = \frac{JT^{1/2}}{GM^{5/2}}, \quad (3)$$

As with the previous definition this  $\lambda$  can be easily calculated numerically. The advantage of this spin parameter is that it can be calculated easily for any shape of the halo. Therefore, this definition is especially suited for the calculation of the spin parameter of halos found with the FOF analysis.

The halos identified in the MareNostrum universe consists of two components, dark matter and gas. Then for each component the spin parameter is the ratio of the angular velocity  $\omega$  of that component to  $\omega_{\text{sup}}$  of the system. Therefore, we have

$$\lambda_{\text{gas(DM)}} = \frac{J_{\text{gas(DM)}}}{M_{\text{gas(DM)}} (2G(M_{\text{gas}} + M_{\text{DM}}) R_{\text{vir}})^{1/2}}, \quad (4)$$

where  $M_{\text{gas(DM)}}$  denote the gas (DM) mass inside the virial sphere of radius  $R_{\text{vir}}$  and  $J_{\text{gas(DM)}}$  the angular momentum of the corresponding component. Note, that we

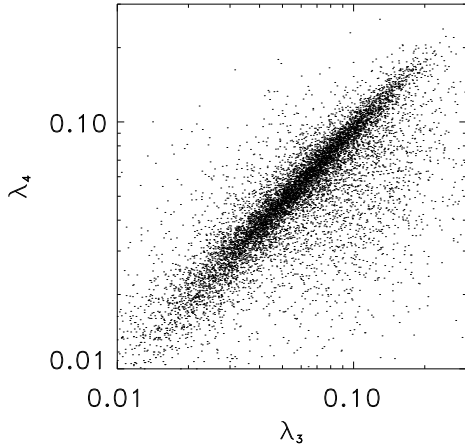


FIG. 3.— Comparison of the DM spin parameter  $\lambda_3$  calculated according to Eq. (3) and  $\lambda_4$  computed from Eq. (4)

have introduced in Eq.(4) an additional quotient of  $\sqrt{2}$  to be consistent with the definition of Bullock et al. (2001).

van den Bosch et al. (2002) and Sharma & Steinmetz (2005) discussed in detail the angular momentum distributions of the gas and dark matter components of halos found in SPH cosmological simulations. To this end they decomposed the particle velocities into a streaming and a random component. The velocities of the SPH gas particles are streaming velocities to which one could add microscopic random motions. The velocities of the DM particles contain random motions which could be eliminated by smoothing over a certain interpolation kernel. Nevertheless, as long as the number of particles in the halo is very large compared to the number of smoothing neighbors the effects of the smoothing on the spin parameter can be neglected (Sharma: private communication). Following Sharma & Steinmetz (2005) we use the total velocities of the DM and gas particles as provided by the simulation to calculate the spin parameters of both components.

We want to compare the spin parameters of a given structure calculated by the different abovementioned definitions. The objects found by the FOF algorithm have arbitrary shapes and the spin parameter as defined in Eq. (3),  $\lambda_3$  is calculated with respect to the center of mass of each object. On the other hand, we have also calculated the spin parameter for spherical halos at virial overdensity ( $334 \times$  mean density at redshift  $z = 0$ ). In this case, we first identify for each of the FOF objects the highest density peak. To this end, we decrease the linking length by a factor of 8 ending up with sub-structures of about  $170,000 \times$  mean density. For each FOF object we take the center of mass of the most massive sub-structure as the center of a sphere and determine the virial radius and mass within this sphere. Then we use Eq. (4) to calculate the DM spin parameter  $\lambda_4$ . In Fig. 3 we compare the DM spin parameters  $\lambda_3$  and  $\lambda_4$ . Having in mind the completely different treatments of the spin parameter they agree surprisingly well. More than 63 % of our halos are within 20 % scatter around the  $\lambda_3 = \lambda_4$  relation. The reason for the larger deviations shown in this plot is due to the fact that halos defined from the spherical overdensity criterium and those defined from FOF

algorithm look completely different if substructures are present. In such cases, the spin of the FOF objects is calculated with respect to the center of mass whereas for the spherical halos it is calculated with respect to the position of the highest density peak. These positions, and the corresponding spins may differ substantially. For those halos in which this effect is not important, the spin parameters defined by both methods have very similar values. However, there is also another source of scatter, although much smaller than the previous one, due to the assumption of virial equilibrium  $2T + U = 0$  which is not exactly fulfilled in our halos. Thus, even for spherical objects the spins  $\lambda_3$  and  $\lambda_4$  will not be identical. In fact, Shapiro et al. (2004) pointed out that the presence of infalling matter acts as a surface pressure even for collisionless DM. The surface term leads to  $2T + U > 0$ . The spin parameter calculated from the kinetic energy,  $\lambda_3$  tends to be slightly larger than the spin parameter  $\lambda_4$ , probably because the total kinetic energy of DM particles is larger than that assumed by virial equilibrium. Hetzner & Burkert (2006) have studied the distribution of the virial coefficient  $\eta = 2T/|U|$  for a sample of dark matter halos from  $\Lambda$ CDM N-body simulations and showed that the mean value of  $\eta$  approaches unity at redshift  $z = 0$ .

In § 3 we found different shapes (and therefore volumes) for the DM and gas components of the halos. Therefore, to compare the spin parameter of both components we better used  $\lambda$  defined by Eq. 4. We put a sphere at the position of the most massive substructure as described above and determine the virial radius and mass of the halo as well as the gas and dark matter masses (see § 5) and the corresponding angular momenta.

The resulting distribution of the spin parameter of the gas and dark matter components are shown in Fig. 4. The distribution of the spin parameter  $\lambda$  can be described by a log-normal distribution

$$P(\lambda) = \frac{1}{\sqrt{2\pi}\sigma_\lambda\lambda} \exp \left[ -\frac{\ln^2(\lambda/\lambda_0)}{2\sigma_\lambda^2} \right]. \quad (5)$$

The best fit parameters are for the DM distribution  $\lambda_0 = 0.0351 \pm 0.0016$ ,  $\sigma_\lambda = 0.6470 \pm 0.0067$  and for the gas distribution  $\lambda_0 = 0.0462 \pm 0.0012$ ,  $\sigma_\lambda = 0.6086 \pm 0.0030$ .  $P(\lambda)$  has a maximum at  $\lambda_{max} = 0.0231$ ,  $0.0319$  for the DM resp. gas distribution. Recently, Bett et al (2006) have proposed another distribution function which fits their data better. Since the scatter of  $\lambda_0$  with varying total number of halos depending on the lower mass cut-off is in our case of the same order as the error in the determination of  $\lambda_0$  we believe that the log-normal function is a sufficient fit to describe the behavior of the spin parameter. The differences of  $\lambda_0$  using different definitions of  $\lambda$  are at least of the same order.

Since dark matter dominates the total mass the total distribution of the spin parameter of dark matter and gas practically coincides with that of the dark matter only. Moreover, it is in agreement with the distribution of the spin parameter calculated by Gottlöber et al. (2006a) using Eq.(3) for the non-spherical FOF halos.

van den Bosch et al. (2002) found agreement between the spin distribution of the gas and DM components of 378 halos identified in a small box of  $10h^{-1}\text{Mpc}$  at redshift  $z = 3$ . We see a substantial shift of the log-normal distribution of the gas spin towards higher

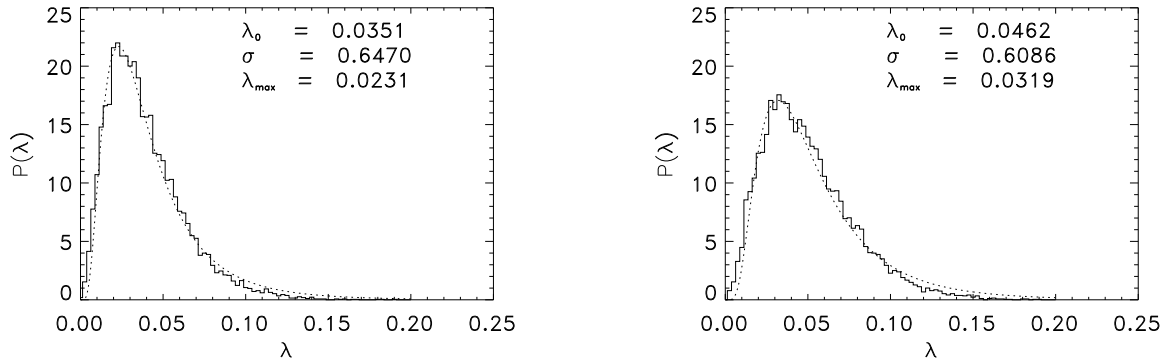


FIG. 4.— *Left*: Distribution of the spin parameter of the dark matter in halos with masses larger than  $5 \times 10^{13} h^{-1} M_{\odot}$ . The dotted line is a log-normal distribution Eq.(5) with the parameters  $\lambda_0$  and  $\sigma$  as given in the plot. *Right*: The same for the spin parameter of the gas in halos.

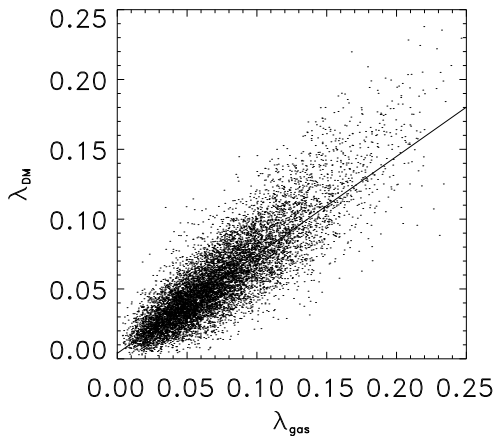


FIG. 5.— Distribution of the spin parameter of the gas and DM components. The solid line is the Least Square linear fit  $\lambda_{DM} = 0.72\lambda_{gas} + 0.004$ .

spin in comparison to the dark matter. Our  $\lambda_0$  are slightly larger than the values (0.0287, 0.0412) reported by Sharma & Steinmetz (2005) for a sample of 41 halos in a box of  $32.5 h^{-1} \text{Mpc}$  at redshift  $z = 0$ . We find a mean  $\lambda_{gas}/\lambda_{DM}$  of 1.39 (see Fig. 5) with a tendency to decrease with halo mass. The standard deviation is 0.57. Only the 159 most massive halos ( $M_{vir} > 5 \times 10^{14} h^{-1} M_{\odot}$ ) show a substantially smaller  $\lambda_{gas}/\lambda_{DM} = 1.23$  with a standard deviation of 0.45.

At  $z = 1$  we found a similar behavior of the spins of the DM and gas components. Both spins follow log-normal distributions which can be described by  $\lambda_0 = 0.0467$  and  $0.0541$  respectively, *i.e.* the mean spin of the gas component is 1.16 times larger than the spin of the DM component. During further evolution this ratio increases until 1.39. The spins themselves are slightly larger at redshift  $z = 1$ .

## 5. BARYON FRACTION

The observed cluster baryon fraction is an important tool for the determination of cosmological parameters. Typically the gas fraction in clusters is measured by X-ray observations at overdensities 500 or larger, *i.e.* well inside the virial radius. A certain fraction of the baryons reside in stars. Using a non-radiative simulation to deter-

mine the baryon fraction is by sure a simplification, but since we are interested in the baryon fraction at virial radius we expect not to be affected very much by neglecting cooling and star formation processes (see the discussion below).

During the last decade baryon fractions in clusters  $Y_b = f_{cluster}/f_{cosmic} = f_{cluster}/(\Omega_b/\Omega_{matter})$  have been studied in non-radiative simulation by several authors. Eke, Navarro, & Frenk (1998) found within the virial radius a baryon fraction of  $0.85 - 0.9$ . Within the Santa Barbara cluster comparison project (Frenk et al. 1999) the baryon fraction at virial radius averaged over all codes was  $Y_b = 0.92$ . They found a substantial scatter between codes and a systematic offset between SPH and grid codes which led to higher baryon fractions. Recently, Kravtsov, Nagai, & Vikhlinin (2005) found that at large radii the baryon fraction in the ART simulations is by about 3% – 5% higher than in GADGET simulations of the same clusters. Within our non-radiative simulation we have explored the baryon fraction at the virial radius in objects with virial masses larger than  $5 \times 10^{13} h^{-1} M_{\odot}$ . The assumed virial overdensity at redshift  $z = 0$  is 334, at redshift  $z = 1$  it is 201. At redshifts  $z = 0$  we found more than 10000 objects and about 2500 at redshift  $z = 1$ . The scatter in the measured baryon fraction of our cluster was found to be quite large. At redshift  $z = 0$  it ranges between 0.85 and 1.0 with a mean of 0.92 (Gottlöber et al. 2006a).

In Fig. 6 we show the ratio  $Y_b$  as a function of the virial mass of clusters. Due to the large number of objects the standard deviation of the mean value of  $Y_b$  for different mass bins is small and we could fit a linear relation in the semi-logarithmic plot,  $Y_b = \alpha \ln(M) + \beta$ , with the slope  $\alpha = -0.005 \pm 0.001$  at redshift  $z = 0$  and  $\alpha = -0.006 \pm 0.001$  at redshift  $z = 1$ . There is a 2% decrease of the baryon fraction between redshifts one and zero. Ettori et al. (2006) found 5 % decrease of the baryon fraction in this time interval. Within our model the decrease can be naturally expected. Since the gas works against its pressure during the formation of the cluster the total dark matter mass grows slightly faster than the gas mass. Therefore, the relative gas fraction decreases with time as can be seen in Fig. 6. For illustration we have selected 1200 clusters with masses larger than  $2 \times 10^{14} h^{-1} M_{\odot}$  and 2900 clusters with masses smaller than  $2 \times 10^{14} h^{-1} M_{\odot}$  and compared the mass growth of

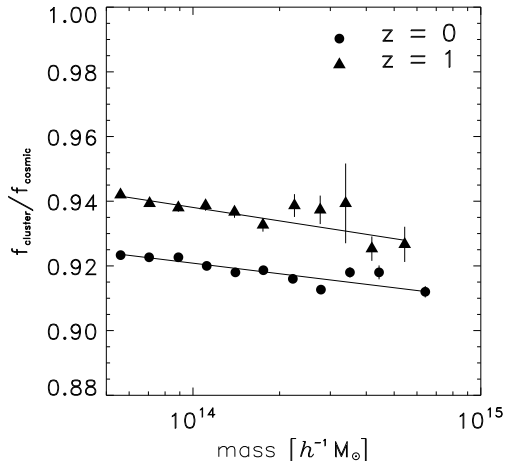


FIG. 6.— Baryon fraction, normalized to the cosmic baryon fraction, in clusters as a function of halo mass for two different redshifts.

their DM and baryonic components between  $z = 0$  and  $z = 1$ ,  $D_{DM,gas} = m_{DM,gas}(z = 0)/m_{DM,gas}(z = 1)$ . The averaged relative growth  $D_{DM}/D_{gas}$  is 1.03 for  $M > 2 \times 10^{14} h^{-1} M_{\odot}$  and 1.02 for  $M < 2 \times 10^{14} h^{-1} M_{\odot}$ , i.e. clusters accrete DM faster than gas and the mean baryonic fraction decreases with time. Originally the baryon fraction was homogenous. During collapse of the whole cluster region the baryonic fraction decreases slowly. Most massive clusters are situated in the positions of the highest density peaks in the originally almost homogenous medium. These peaks start to grow first. This could be the reason for small but statistically significant slope  $\alpha$  which we found. Note, however, that recently Crain et al. (2006) have found the opposite, a slightly increasing baryon fraction with mass, from a set of clusters extracted from a non-radiative SPH resimulation of the Millenium Run, but with 2 times less number of particles than ours. Also, the relative baryon fraction of their clusters (at overdensity 200) falls below 0.9.

Recently Kravtsov, Nagai, & Vikhlinin (2005) studied the effects of cooling and star formation on the the baryon fractions in clusters. They showed that the cooling of the gas and the associated star formation increases the baryon fraction even at radii as large as the virial radius. The averaged baryon fraction at virial radius differ by 5 % between the simulations with cooling and star formation ( $Y_b = 1.02$ ) and the non-radiative simulations ( $Y_b = 0.97$ ), which is already  $\sim 5$  % larger than the value we obtained from the MareNostrum Universe SPH simulation. Ettori et al. (2006) have also studied a set of clusters obtained both in non-radiative SPH simulations as well as in simulations including cooling and star formation. For the non-radiative simulations they found an averaged baryon fraction of 0.89, which is slightly lower than the value we found. In agreement with Kravtsov, Nagai, & Vikhlinin (2005) they also found in

their simulations with cooling and star formation that the baryon fraction at virial radius increases with respect to the non-radiative case by about 3 %.

## 6. CONCLUSIONS

We have selected a statistically significant sample of more than 10,000 clusters from the MareNostrum universe simulation. With this database we have determined the shape and the spin of the DM and gas components of the clusters independently. We found that both the gas and dark matter components tend to be prolate although the gas is much more spherically distributed. The mean ratio of the minor to major axis decreases with increasing halo mass, i.e. younger objects tend to be less spherical, in agreement with the results of Kasun & Evrard (2005) obtained from the Hubble Volume DM only simulation. On the other hand, the triaxiality parameters of the gas and DM component differ by a few percent only and both of them increase with halo mass.

The spin parameters of the DM and gas components are well represented by lognormal distribution functions with  $\lambda_0 = 0.0351$  (DM) and  $\lambda_0 = 0.0462$  (gas). These values are slightly larger than the values found for a sample of 41 halos with masses from dwarf to bright galaxies (Sharma & Steinmetz 2005). On average, the spin of the gas component is by a factor of 1.39 larger than the spin of the DM component. This ratio is smaller for very massive halos, 1.23 for halos with  $M_{vir} > 5 \times 10^{14} h^{-1} M_{\odot}$ . It decreases slightly with redshift being 1.16 at  $z = 1$ .

On average, the baryon fraction in the cluster sample is  $Y_b = 0.92$ . The baryon fraction increases with redshift, being 0.94 at  $z = 1$ . At both redshift the baryon fraction decreases slightly with increasing virial mass of the clusters. The radiative processes of cooling and star formation are expected to change the baryon content found for halos in non-radiative simulations. There is a discrepancy between the predicted baryon fraction in SPH and AMR codes. Both effects are of the same order as the time and mass dependence found here. Thus, at present observational projects to estimate cosmological parameter such as the total matter density in the universe and the equation of state of the dark energy can still safely assume a rather universal, unevolving baryon fraction for clusters of galaxies.

## ACKNOWLEDGMENTS

The MARENOSTRUM UNIVERSE has been created at the Barcelona Supercomputer Center and analyzed at NIC Jülich. We thank Acciones Integradas Hispano-Alemanas and DFG for financial support. GY would like to thank also MCyT for financial support under project numbers AYA2003-07468 and BFM2003-01266. We appreciate very much the fruitful discussions with S. Sharma, M. Hoeft, M. Steinmetz and A. Knebe. We would also like to thank the anonymous referee for her/his valuable comments on the first version of the paper.

## REFERENCES

Allgood B., Flores R. A., Primack J. R., Kravtsov A. V., Wechsler R. H., Faltenbacher A., Bullock J. S., 2006, MNRAS, 367, 1781  
 Ascasibar Y., Sevilla R., Yepes G., Müller V., Gottlöber S., 2006, MNRAS, 371, 193

Avila-Reese V., Colín P., Gottlöber S., Firmani C., Maulbetsch C., 2005, ApJ, 634, 51  
 Bailin J., Steinmetz M., 2005, ApJ, 627, 647  
 Binney J., 1985, MNRAS, 212, 767

- Basilakos S., Plionis M., Yepes G., Gottlöber S., Turchaninov V., 2006, *MNRAS*, 365, 539
- Bett Ph., Eke V., Frenk C.S., Jenkins A., Helly J., Navarro J., [astro-ph/0608607](#)
- Bullock J. S., Dekel A., Kolatt T. S., Kravtsov A. V., Klypin A. A., Porciani C., Primack J. R., 2001, *ApJ*, 555, 240
- Chen D. N., Jing Y. P., Yoshikaw K., 2003, *ApJ*, 597, 35
- Crain R. A., Eke V. R., Frenk C. S., Jenkins A., McCarthy I. G., Navarro J. F., Pearce F. R., 2006, *astro*, [arXiv:astro-ph/0610602](#)
- Eke V. R., Navarro J. F., Frenk C. S., 1998, *ApJ*, 503, 569
- Ettori S., Dolag K., Borgani S., Murante G., 2006, *MNRAS*, 365, 1021
- Faltenbacher A., Allgood B., Gottlöber S., Yepes G., Hoffman Y., 2005, *MNRAS*, 362, 1099
- Faltenbacher A., Hoffman Y., Gottlöber S., Yepes G., 2006, [astro-ph/0608304](#)
- Frenk C. S., et al., 1999, *ApJ*, 525, 554
- Gottlöber S., Yepes G., Wagner C., Sevilla R., 2006a, *Proceedings of the XLlst Rencontres de Moriond, XXVIth Astrophysics Moriond Meeting: From Dark Halos to Light*, Eds. Tresse L., Maurogordato S., Tran Than Van J., [astro-ph/0608289](#)
- Gottlöber S., Yepes G., Khalatyan A., Sevilla R., Turchaninov V., 2006b, *Proceedings of the DSU2006 conference*, Eds. Munoz C., Yepes G., American Institute of Physics, [astro-ph/0610622](#)
- Hetznecker H., Burkert A., 2006, *MNRAS*, 370, 1905
- Kasun S. F., Evrard A. E., 2005, *ApJ*, 629, 781
- Klypin A., Gottlöber S., Kravtsov A. V., Khokhlov A. M., 1999, *ApJ*, 516, 530
- Klypin A., Kravtsov A. V., Bullock J. S., Primack J. R., 2001, *ApJ*, 554, 903
- Kravtsov A. V., Nagai D., Vikhlinin A. A., 2005, *ApJ*, 625, 588
- Macciò A., Dutton A., van den Bosch F., Moore B., Potter D., Stadel J., [astro-ph/0608157](#)
- Padmanabhan, T., 1993, *Structure formation in the universe* (Cambridge: Cambridge University Press)
- Peebles P. J. E., 1971, *A&A*, 11, 377
- Shapiro P. R., Iliev I. T., Martel H., Ahn K., Alvarez M. A., 2004, *astro*, [arXiv:astro-ph/0409173](#)
- Sharma S., Steinmetz M., 2005, *ApJ*, 628, 21
- Springel V., 2005, *MNRAS*, 364, 1105
- van den Bosch F. C., Abel T., Croft R. A. C., Hernquist L., White S. D. M., 2002, *ApJ*, 576, 21
- Vitvitska M., Klypin A. A., Kravtsov A. V., Wechsler R. H., Primack J. R., Bullock J. S., 2002, *ApJ*, 581, 799
- Yepes G., Ascasibar Y., Sevilla R., Gottlöber S., Müller V., 2004, *Proceedings of IAU Colloquium 195 "Outskirts of Galaxy Clusters: Intense Life in the suburbs"*, Ed. A. Diaferio, Cambridge Univ. press, pag. 274.